JOURNAL OF THERMOPHYSICS AND HEAT TRANSFER
Vol. 17, No. 1, January–March 2003

Short-Time Thermal Effects on Thermomechanical Response Caused By Pulsed Lasers

J. K. Chen,* J. E. Beraun,* and L. E. Grimes*
U.S. Air Force Research Laboratory, Kirtland Air Force Base, New Mexico 87117
and
D. Y. Tzou†
University of Missouri—Columbia, Columbia, Missouri 65211

An ultrafast thermoelasticity model is proposed to analyze the heat transport and thermomechanical phenomena in metal films heated by femtosecond laser pulses. It covers 1) the dual-hyperbolic two-step heating process in thermal transport, 2) the hot-electron blast effect in momentum transfer, 3) the coupling effect between lattice temperature and strain rate, 4) the thermal stress relaxation effect, and 5) the volumetric absorption of laser beam energy. The coupled transient thermoelasticity equations are solved with a nonconventional finite difference scheme. Numerical analysis is performed for gold films under the conditions of uniaxial strain and uniaxial stress, respectively. The effects of the heat-flux relaxations in electrons and the lattice, thermal stress relaxation, hot-electron blast force, and thermal-mechanical coupling are investigated.

Nomenclature

A_e, B_l	=	constants in electron relaxation time
B	=	hot electron blast force
C	=	heat capacity
G	=	electron–phonon coupling factor
g	=	nondimensional electron–phonon coupling factor
J_0	=	laser fluence
K	=	thermal conductivity
q	=	heat flux
R	=	surface reflectivity
S	=	volumetric heat source
T	=	temperature
T_0	=	initial (reference) temperature
t	=	time
t_p	=	laser pulse duration
u	=	displacement
V_s	=	speed of sound
$X_{,i}$	=	$\partial X/\partial x_i$
$\dot{X}$	=	$\partial X/\partial t$
$\ddot{X}$	=	$\partial^2 X/\partial t^2$
x	=	spatial coordinate
x_s	=	optical penetration depth (skin depth)
α	=	thermal expansion coefficient
β	=	$4\ell n(2)$, a constant
Δ	=	increment
δ	=	Kronecker delta
ε	=	strain
ϑ	=	temperature ratio to Fermi temperature
Λ	=	constant in hot-electron blast force
λ	=	Lamé constant
μ	=	shear modulus
Π	=	artificial viscosity
ρ	=	mass density
σ	=	stress
τ	=	relaxation time
χ, η	=	constants in electron thermal conductivity
ω_L, ω_q	=	constants in artificial viscosity

Subscripts and Superscripts

e	=	electron
F	=	Fermi
i, j, k	=	components x, y, or z
l	=	lattice (phonon)
s	=	thermal stress

Introduction

BECAUSE of the advantages of much lower fluence needed to accomplish ablation[1–4] and considerably sharper contour being achievable,[2,5–7] research of subpicosecond pulse laser ablation has received great attention in the past decade. Under a localized heating of sufficiently high intensity in an extremely short time interval, plasma is produced, but hydrodynamic motion in the material is negligible.[7] Postexperimental examination shows that a thin layer of material shatters from the heated surface of the bulk material without a clear signature of thermal damage.[2,5–7] It is believed that the ultrafast damage to metals could involve a "cold" (mechanical) destruction as a result of large lattice deformation and/or "hot" destruction from melting and vaporization.[8] To establish guidelines for appropriate beam settings and control the material processing or nondestructive detecting, accurate description of the temperature fields and the thermal stress waves resulting from ultrashort laser heating is of importance.

Numerous theoretical studies have been conducted to investigate thermoelastic waves in metals generated by short-pulsed laser heating. The simplest approach is to solve the classical thermomechanical equations, with or without the consideration of the coupling effect between temperature and strain rate.[9–12] Because this is not a review paper, only typical references are cited in this work. Because the energy equation does not include the thermal inertia term, the classical thermomechanics approach is adequate only for the laser pulse duration longer than a few nanoseconds. When the laser pulse duration is on the order of the phonon (lattice) relaxation time (in a few to tens picoseconds for metals), the non-Fourier

Received 10 December 2001; revision received 3 June 2002; accepted for publication 19 August 2002.

*Laser Effects Research Branch, Directed Energy Directorate, 3550 Aberdeen Avenue SE.

†James C. Dowell Professor, Department of Mechanical and Aerospace Engineering; TzouR@missouri.edu.

effect has to be incorporated so that the temperature field can be properly characterized. To do so, extensions of the classical theory by including the relaxation effects have been proposed, such as 1) Lord and Shulman theory,[13] 2) Green and Lindsay theory,[14] 3) Green and Naghdi theory,[15] 4) Hetnarski and Ignaczak theory,[16] and 5) the dual-phase lag theory.[17] These generalized theories are categorized as hyperbolic thermoelasticity.[18–20] Applications of these hyperbolic thermoelasticity theories can be found in many works.[21–24]

When the laser pulse duration is shorter than the phonon relaxation time or even shorter than the electron relaxation time (in subpicoseconds for metals), the one-temperature hyperbolic thermoelasticity theories often fail to describe the ultrafast heating behaviors. Because the heating time is so short, the metal lattice essentially remains thermally undisturbed during the laser irradiation. Thus, how to apply the laser energy to the material becomes a challenging problem for the one-temperature theories except for the dual-phase lag model.[17] This situation has created a need for a high-fidelity model that can capture the thermal transport behavior and predict the accurate thermomechanical response for ultrafast laser interactions with solid matter.

In fact, ultrafast thermal transport is a two-step, nonequilibrium process.[25] In the first step the incident laser energy is absorbed predominantly by electrons during the photon excitation. This electron-heating process is limited to the optical penetration (skin) depth. During the second step, a portion of the electron thermal energy diffuses, through electrons, into a deeper region of electrons and a part of the electron thermal energy transfers to the neighboring lattice. Because the heat capacity of electrons is about two orders of magnitude smaller than that of a metal lattice, the electrons could shoot up to a very high temperature while the lattice remains cold. The nonequilibrium thermal transport process continues until an equilibrium, steady state establishes.

Picosecond time-resolved x-ray studies have revealed severe lattice expansion in laser-heated thin gold crystal via the shift of the time-dependent x-ray rocking curve,[26,27] which, in essence, motivates the present study. Besides the thermal load resulting from nonuniform lattice temperature, there is another important load generated from nonequilibrium hot electrons,[8] which has not been considered by classical and hyperbolic thermomechanics. This hot-electron blast force is found to be linearly proportional to the gradient of electron temperature squared. As a result of the great electron temperature confined in the skin depth (in submicrons for metals), the hot-electron blast force could be considerably large and cause severe lattice deformation.[8,28,29] In this work an ultrafast thermomechanical model is proposed to investigate the heating response of metal films subjected to femtosecond laser pulses. This model modifies the dual-hyperbolic two-temperature theory[30] for describing electron and lattice temperatures and incorporates the hot-electron blast force[8] into the momentum equations for modeling thermomechanical response. It also includes the thermal stress relaxation effect,[14] the thermal-mechanical coupling effect, and the volumetric absorption of laser beam energy. Because of the strongly temperature-dependent thermophysical properties, the coupled time-dependent partial differential equations are solved with a nonconventional finite difference scheme, with which the temperatures and displacements are evaluated at the grid points and the heat fluxes and stresses are calculated at the halfway point location between two grid points. Numerical analysis is performed with gold films under the condition of uniaxial strain but three-dimensional stress and the condition of uniaxial stress but three-dimensional strain, respectively. The effects of the heat-flux relaxations in electrons and the lattice, thermal stress relaxation, hot-electron blast force, and thermal-mechanical coupling are investigated.

Mathematical Formulation

A homogeneous, isotropic, thermoelastic metal material is considered in this work. In the absence of body force, the equations of motion and the energy balance equation in the classical thermoelasticity are given as[31]

$$\rho \ddot{u}_i = \sigma_{ji,j} \tag{1}$$

$$C\dot{T} = -q_{k,k} - (3\lambda + 2\mu)\alpha T_0 \dot{\varepsilon}_{kk} + S \tag{2}$$

with the constitutive laws for stress and heat flux,

$$\sigma_{ij} = 2\mu\varepsilon_{ij} + \lambda\varepsilon_{kk}\delta_{ij} - (3\lambda + 2\mu)\alpha(T - T_0)\delta_{ij} \tag{3}$$

$$q_i = -KT_{,i} \tag{4}$$

as well as the strain-displacement relations,

$$\varepsilon_{ij} = \tfrac{1}{2}(u_{i,j} + u_{j,i}) \tag{5}$$

The repeated index represents summation. The comma and overdot denote derivatives with respect to the spatial coordinate and time, respectively.

For an ultrashort laser heating process the phenomena of thermal and momentum transfers are different from those described by the preceding classical thermomechanics. In fact, the ultrafast thermal transport is a two-step process, as mentioned earlier. To describe the thermal transport behavior, several two-step heating models, which are able to characterize the electron and lattice temperatures in metals, have been proposed.[25,30,32] Among which, the most general, dual-hyperbolic two-temperature model[30] is modified in this study.

Because the heating process takes place in such a short time period, it is expected that the thermodynamic states have no sufficient time to achieve equilibrium before they move on in the time history. Two of the natural consequences from the nonequilibrium process, which are of interest here, are on the heat-flux vector and the deviatoric stress tensor.[17] By taking into account the lagging effects, the constitutive equations for heat flux[13] and thermal stress[14] become

$$\tau\dot{q}_i + q_i = -KT_{,i} \tag{6}$$

$$\sigma_{ij} = 2\mu\varepsilon_{ij} + \lambda\varepsilon_{kk}\delta_{ij} - (3\lambda + 2\mu)\alpha[(T - T_0) + \tau_s\dot{T}]\delta_{ij} \tag{7}$$

where τ and τ_s are the relaxation times for the heat flux and thermal stress, respectively. Another important physical phenomenon, which is excluded in the classical and hyperbolic models of thermoelasticity, is the hot-electron blast force B_i. It is generated from nonequilibrium hot electrons and derived recently by Falkovsky and Mishchenko,[8] based on the complete Lagrangian describing the phonon–electron interactions in the picosecond domain:

$$B_i = \Lambda T_{,i}^2 \tag{8}$$

where Λ is estimated to be gC_{eo} with $g \sim 1$ denoting the dimensionless electron–phonon coupling constant and C_{eo} being a constant characteristic in the temperature-dependent electron heat capacity[33]

$$C_e = C_{eo}T_e \tag{9}$$

The hot-electron blast force exerts on the lattice, in addition to the thermomechanical load caused by the temperature gradient established across the lattice. Renormalization of elastic moduli is another short-time effect caused by electron looping in the phonon (lattice) self-energy function. The resulting changes in elastic properties, however, are of the order of $(T_e/T_F)^2$, with T_F being the Fermi temperature. Unless the laser power is extremely high and electrons become highly excited, so that $T_e \sim T_F$, such an effect of lattice renormalization is usually less than 1% and neglected.[8,28]

To describe the thermomechanical response of metals irradiated by an ultrashort laser pulse, a complete model, as aforementioned, should include 1) the volumetric absorption of laser beam energy, 2) the nonequilibrium thermal transport,[25,30,32] 3) the coupling effect between lattice temperature and strain rate, 4) the hot-electron blast force,[8] and 5) the lagging effects on the heat flux[13] and thermal stress.[14] Thus, a set of the one-dimensional governing equations for ultrafast thermoelasticity is proposed:

$$\rho_l \ddot{u}_x = \sigma_{xx,x} + 2\Lambda T_e T_{e,x} \tag{10}$$

$$C_e\dot{T}_e = -q_{\mathrm{ex},x} - G(T_e - T_l) + S(x,t) \tag{11}$$

$$\tau_e\dot{q}_{\mathrm{ex}} + q_{\mathrm{ex}} = -K_e T_{e,x} \tag{12}$$

$$C_l\dot{T}_l = -q_{\mathrm{lx},x} + G(T_e - T_l) - (3\lambda + 2\mu)\alpha T_l\dot{\varepsilon}_{kk} \tag{13}$$

$$\tau_l\dot{q}_{\mathrm{lx}} + q_{\mathrm{lx}} = -K_l T_{l,x} \tag{14}$$

with the volumetric laser heat source represented by

$$S(x,t) = \sqrt{\frac{\beta}{\pi}}\frac{(1-R)J_0}{t_p x_s}\exp\left[-\left(\frac{x}{x_s}\right) - \beta\left(\frac{t-2t_p}{t_p}\right)^2\right] \tag{15}$$

The stresses in Eq. (10) are described by Eq. (7) with the thermal stress relaxation. In contrast to the use of surface heat flux in describing frequency-modulated, Q-switched, or mode-locked lasers,[34–37] Eq. (15) describes the energy absorption rate in metals heated by a picosecond laser, including the combined effects of skin-depth x_s, pulse duration t_p, and surface reflectivity R. Equation (15) is employed in this work because it was used in confirming the experimental results for ultrafast heating on thin metal films.[32,38–40]

Equations (11–14) reduce to the dual-hyperbolic two-temperature model[30] if the coupling between temperature and strain rate is dropped off. They further reduce to the hyperbolic two-temperature model[32] by excluding all of the lattice heat-flux-related terms and to the parabolic two-temperature model[25] by further letting the electron relaxation time be zero. Such transition of the two-temperature model in different domains of response time has gained numerous experimental supports in the development of microscale heat transfer.[17,25,32,38–40] Equations (11–14) were derived from the semiclassical Boltzmann transport equation for discrete assemblies.[32] Though bearing the final appearance for a continuum, Eqs. (11–14) capture the unique behaviors of thermal relaxation and rapid thermalization that cannot be depicted by the classical models of Fourier diffusion and thermal waves.[17] The hot-electron blast force, in the momentum equation (10), is an important, new physical phenomenon that the classical and hyperbolic thermoelasticity theories have ignored. Equation (15) indicates that the laser beam is Gaussian in time. It is applied on the front surface ($x = 0$), and the peak intensity occurs when $t = 2t_p$. As the depth increases, the volumetric laser heat source attenuates with an exponential function, $\exp(-x/x_s)$.

Under the uniaxial strain condition

$$\varepsilon_{xx}(x,t) \neq 0, \qquad \varepsilon_{yy} = \varepsilon_{zz} = \varepsilon_{xy} = \varepsilon_{yz} = \varepsilon_{zx} = 0 \tag{16}$$

the three nonzero normal stresses become

$$\sigma_{xx} = (\lambda + 2\mu)\varepsilon_{xx} - (3\lambda + 2\mu)\alpha[(T_l - T_0) + \tau_s\dot{T}_l] \tag{17}$$

$$\sigma_{yy} = \sigma_{zz} = \lambda\varepsilon_{xx} - (3\lambda + 2\mu)\alpha[(T_l - T_0) + \tau_s\dot{T}_l] \tag{18}$$

From Eq. (16) the time rate of change of the lattice dilation $\dot{\varepsilon}_{kk}$ is equal to $\dot{\varepsilon}_{xx}$. Under the uniaxial stress condition

$$\sigma_{xx}(x,t) \neq 0, \qquad \sigma_{yy} = \sigma_{zz} = \sigma_{xy} = \sigma_{yz} = \sigma_{zx} = 0 \tag{19}$$

the only nonzero stress component is

$$\sigma_{xx} = E[\varepsilon_{xx} - \alpha(T_l - T_0 + \tau_s\dot{T}_l)] \tag{20}$$

in which E is the Young's modulus. The time rate of change of the lattice dilation is thus derived

$$\dot{\varepsilon}_{kk} = [(1-2\nu)/E]\sigma_{xx} + 3\alpha(T_l - T_0 + \tau_s\dot{T}_l) \tag{21}$$

where ν is the Poisson's ratio.

The governing equations (10–14) along with the laser heat source, Eq. (15), the stress-strain relations, Eq. (7), and the strain-displacement relations, Eq. (5), will be solved under proper initial and boundary conditions. For simplicity, the following conditions are considered:

$$T_e(x,0) = T_l(x,0) = T_0 \tag{22}$$

$$u_x(x,0) = \dot{u}_x(x,0) = 0 \tag{23}$$

$$\sigma_{xx}(x,0) = \sigma_{yy}(x,0) = \sigma_{zz}(x,0) = 0 \tag{24}$$

$$q_{\mathrm{ex}}(0,t) = q_{\mathrm{ex}}(L,t) = 0 \tag{25}$$

$$q_{\mathrm{lx}}(0,t) = q_{\mathrm{lx}}(L,t) = 0 \tag{26}$$

$$\sigma_{xx}(0,t) = \sigma_{xx}(L,t) = 0 \tag{27}$$

where L is the film thickness. In this study T_0 is set at 300 K (room temperature). For uniaxial stress the two initial conditions for stresses σ_{yy} and σ_{zz} in Eq. (24) are discarded.

Three thermophysical properties of electrons involved in the present ultrafast thermoelasticity model are strongly temperature sensitive. They are the electron heat capacity [Eq. (9)], relaxation time, and thermal conductivity. The electron relaxation time is characterized by the electron and lattice temperatures[41]

$$\tau_e = 1\Big/\left(A_e T_e^2 + B_l T_l\right) \tag{28}$$

in which A_e and B_l are constants. The electron thermal conductivity is expressed in the form[42]

$$K_e = \chi\frac{\left(\vartheta_e^2 + 0.16\right)^{\frac{5}{4}}\left(\vartheta_e^2 + 0.44\right)\vartheta_e}{\left(\vartheta_e^2 + 0.092\right)^{\frac{1}{2}}\left(\vartheta_e^2 + \eta\vartheta_l\right)} \tag{29}$$

where $\vartheta_e = T_e/T_F$ and $\vartheta_l = T_l/T_F$ are the normalized electron and lattice temperatures; χ and η are constants. The electron relaxation time, Eq. (28), and the electron thermal conductivity, Eq. (29), are suitable for a wide range of temperatures, from room temperature to the Fermi temperature. On the other hand, the phonon relaxation time τ_l is less temperature sensitive and is given by[17]

$$\tau_l = 3K_l\Big/C_l V_s^2 \tag{30}$$

Note that some of the properties of a metal lattice have been assumed independent of temperature, whereas the temperature-dependent properties are particularly addressed in electrons. Indeed, electrons are much more sensitive to temperature than phonons during the picosecond transient, which is a behavior confirmed in several experimental results.[25,32,38–40]

Solution Algorithm

Because of the mathematical complexity of the coupled governing equations, it is impossible to derive closed-form solutions to the present ultrafast thermoelasticity model. Therefore, Eqs. (10–14) are solved with a finite difference method. Uniform grid meshes are employed. For the spatial derivatives the central difference scheme is used to approximate the quantities at the interior points, and the forward difference scheme is used to estimate the quantities at the boundary.

Like the conventional finite difference, all of the variables are evaluated at the grid points. It is found that the temperatures and stress computed with this approach exhibit a local fluctuation. To improve the serrations, an alternate algorithm is proposed here, with which the electron and lattice temperatures as well as the displacement are calculated at the grid points (same as the conventional method), whereas the heat fluxes and stress are evaluated at the halfway point location between two consecutive grid nodes. At the boundary the temperatures, heat fluxes, and stress are solved where they are unknown and are directly imposed where they are specified. The finite difference grid points used in the present algorithm are sketched in Fig. 1. For convenience, this approach is referred as the QS-point method.

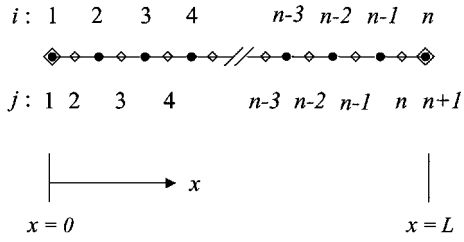

Fig. 1 Finite different grid points for the QS-point method.

For wave propagation problems solved with finite difference methods, the numerical solutions often exhibit spurious (V-shape) oscillation.[43,44] To further suppress the minor oscillation in thermomechanical response, an artificial viscosity[44] is introduced,

$$\Pi = \omega_L \rho_l V_s \Delta x \left| \frac{\partial \dot{u}_x}{\partial x} \right| - \rho_l (\omega_Q \Delta x)^2 \left| \frac{\partial \dot{u}_x}{\partial x} \right| \frac{\partial \dot{u}_x}{\partial x} \qquad (31)$$

in which the two constants $\omega_L = 0.05$ and $\omega_Q = 2.0$ are employed. Thus, the momentum equation (10) is modified to

$$\rho \ddot{u}_x = \sigma_{xx,x} + 2\Lambda T_e T_{e,x} + \Pi_{,x} \qquad (32)$$

Once all of the first spatial derivatives of the temperatures T_e and T_l, heat fluxes q_{ex} and q_{lx}, and stress σ_{xx} are computed, the time rates $\dot{T}_e$, $\dot{T}_l$, $\dot{q}_{ex}$, $\dot{q}_{lx}$, and the acceleration $\ddot{u}_x$ can be determined from Eqs. (10–14) accordingly. The current values of T_e, T_l, q_{ex}, q_{lx}, and u_x are then advanced using a forward difference. For instance, the electron temperature is updated with

$$T_e(x_i, t + \Delta t) = T_e(x_i, t) + \dot{T}_e(x_i, t)\Delta t \qquad (33)$$

where Δt is a time increment. As the values of system parameters vary in presence of uniaxial strain and uniaxial stress as well as a finite thickness of the film, the present algorithm is more stable than our previous method.[29]

Results and Discussion

The laser beam considered throughout this section has a pulse width $t_p = 100$ fs and a fluence $J_0 = 4000$ J/m^2, unless mentioned otherwise. Four gold films with thicknesses of 50, 100, 200, and 400 nm are investigated. The temperature-dependent thermal conductivity[45] and the heat capacity of the gold lattice are listed in Table 1. The values in the parentheses are the bulk heat capacity C,[46] and C_l is calculated using the relationship $C = C_e + C_l$. A linear variation is assumed for the properties between any two consecutive data given in Table 1. The other thermophysical properties of gold employed are as follows[32,41,42]: $\rho_l = 1.93 \times 10^4$ kg/m^3, $C_{eo} = 70$ Jm^{-3}K^{-2}, $G = 2.6 \times 10^{16}$ Wm^{-3}K^{-1}, $R = 0.93$, $x_s = 15.3$ nm, $\chi = 353$ Wm^{-1}K^{-1}, $\eta = 0.16$, $T_F = 6.42 \times 10^4$ K, $A_e = 1.2 \times 10^7$ K^{-2}s^{-1}, and $B_l = 1.23 \times 10^{11}$ K^{-1}s^{-1}. The reflectivity of 0.93 and the optical penetration depth of 15.3 nm are the typical values for visible light. With the preceding constants the calculated electron relaxation time is 26.3 fs at room temperature and 0.02 fs at the Fermi temperature, and the phonon relaxation time is about 38.7 ps at room temperature according to Eqs. (28) and (30), respectively. The mechanical properties used are $E = 74.9$ GPa, $\nu = 0.42$, and $\alpha = 14.2 \times 10^{-6}$ m/mK.[47]

The numerical analyses in this section are performed with the uniaxial strain condition, except for the results shown in the last two figures, which are simulated with the uniaxial stress condition for the comparison purpose. In all of the calculations, the thermal stress relaxation effect is deactivated except that the effect itself is studied. On the other hand, all of the other effects, such as the electron and phonon relaxations, the thermal-mechanical coupling, and the hot-electron blast force, are activated unless each individual

Table 1 Conductivity and heat capacity of gold lattice

T, K	K_l, W/mK[a]	C_l (10^6 J/m^{3}K)
300	315	2.479 (2.50)[b]
604	——	2.708 (2.75)
636	271	——
964	246	——
1017	——	2.839 (2.91)
1100	234	——
1137	176	——
1373	——	2.726 (2.82)

[a] Touloukian et al.[45]
[b] Values in the parentheses are the bulk property.[46]

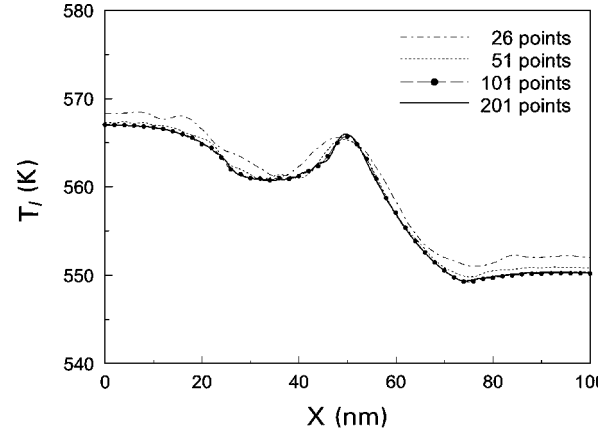

Fig. 2 Convergence study for lattice temperature in a 100-nm gold film heated by a laser pulse with $t_p = 100$ fs and $J_0 = 1000$ J/m^2.

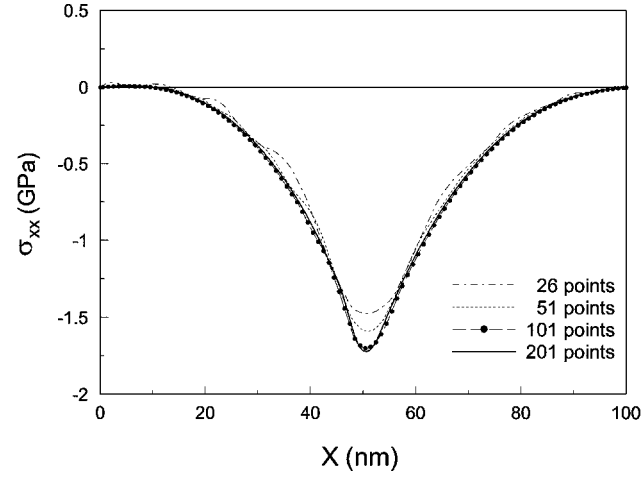

Fig. 3 Convergence study for stress σ_{xx} in a 100-nm gold film heated by a laser pulse with $t_p = 100$ fs and $J_0 = 1000$ J/m^2.

effect itself is investigated. The numerical convergence of the grid mesh models and the film thickness effect on the ultrafast thermomechanical response are examined for the four films, whereas the short-time thermal effects are studied only for the 100-nm film.

The convergence of the grid mesh models is first tested for the QS-point method. The value of J_0 applied is 1000 J/m^2. For brevity, only the lattice temperature T_l and stress σ_{xx} in the 100-nm film are presented here. The results shown in Figs. 2 and 3 are obtained from the four models consisting of 26, 51, 101, and 201 grid points at the time instant when the lattice temperature at the front surface ($x = 0$) reaches the first maximum value (at $t = 15.4 \sim 16.0$ ps, depending on the grid mesh). As seen in Figs. 2 and 3, the solutions computed with the 101 and 201 points are in good agreement, whereas the two coarser models of 26 and 51 points vary noticeably from the two finer models. Form the tests with the four different films,

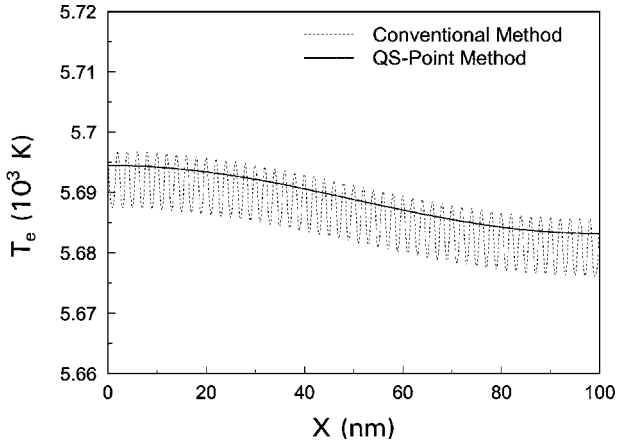

Fig. 4 Electron temperature distribution at $t = 10$ ps in a 100-nm gold film heated by a laser pulse with $t_p = 100$ fs and $J_0 = 4000$ J/m^2, obtained from the conventional finite difference and QS-point methods.

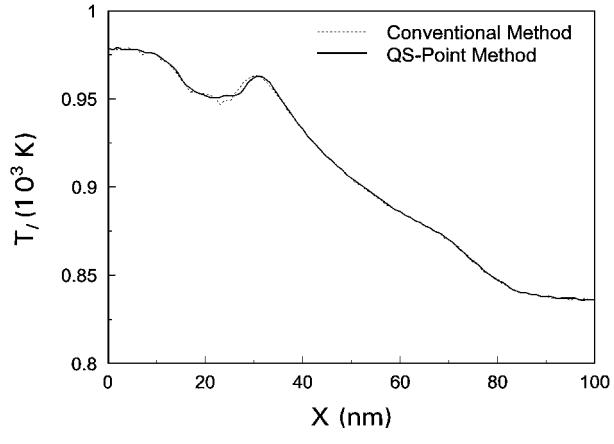

Fig. 5 Lattice temperature distribution at $t = 10$ ps in a 100-nm gold film heated by a laser pulse with $t_p = 100$ fs and $J_0 = 4000$ J/m^2, obtained from the conventional finite difference and QS-point methods.

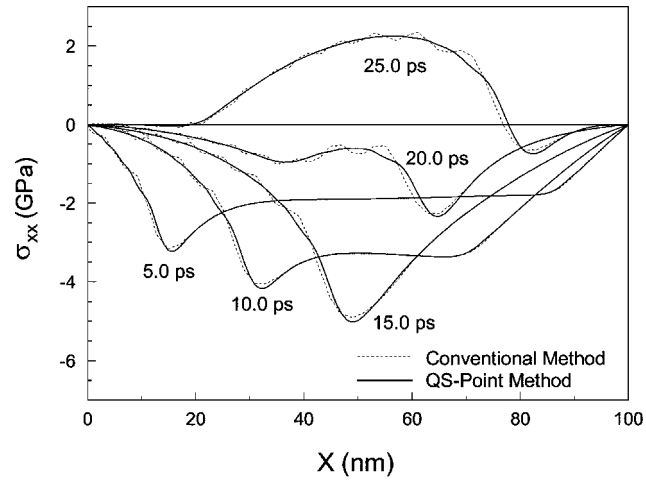

Fig. 6 Stress σ_{xx} distribution at different time instants in a 100-nm gold film heated by a laser pulse with $t_p = 100$ fs and $J_0 = 4000$ J/m^2, obtained from the conventional finite difference and QS-point methods.

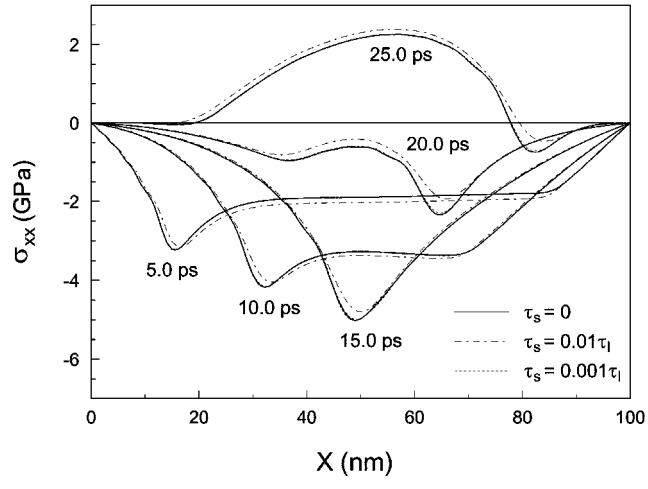

Fig. 7 Effect of thermal stress relaxation on stress σ_{xx} in a 100-nm gold film heated by a laser pulse with $t_p = 100$ fs and $J_0 = 4000$ J/m^2.

generally speaking, a model with one grid point per nanometer is fine enough to result in a reasonably accurate solution. Therefore, the numbers of the grid points employed in the following analysis are 51, 101, 201, and 401 for the 50-, 100-, 200-, and 400-nm films, respectively.

Figures 4–6 compare the performance between the conventional finite difference and QS-point methods. The numerical analysis is performed with the 100-nm film. Artificial viscosity is not used in the conventional finite difference calculation. For clarity, the electron and lattice temperature distributions presented in Figs. 4 and 5 are for one time instant at $t = 10$ ps. It appears, from Fig. 4, that the electron temperature obtained from the conventional finite difference approach exhibits local fluctuation with an amplitude of about 5 K over the entire film thickness. On the other hand, the QS-point result is quite smooth. The minor oscillation about the QS-point solution is also found in the lattice temperature, especially in the region of $x = 0 \sim 30$ nm (see Fig. 5). The results in Figs. 4 and 5 indicate that the lattice temperature is only about one-sixth of the electron temperature. The large difference between the two temperatures reveals that the thermal state at 10 ps is not yet in equilibrium. Figure 6 plots the stress σ_{xx} at five time instants: 5, 10, 15, 20, and 25 ps. Again, the stress solutions obtained from the conventional approach oscillate about those obtained from the QS-point method.

Because the value of the thermal stress relaxation time τ_s is not available, the impact of the thermal stress relaxation on the ultrafast thermomechanical response is studied numerically. It is found that τ_s must be at least one order lower than τ_l, or the numerical solution becomes unstable. For instance, the solution diverges when $\tau_s \geq 0.03\tau_l$. Figure 7 shows the influence of the thermal stress relaxation on stress σ_{xx} for the two relaxation times $\tau_s = 0.01\tau_l$ and $0.001\tau_l$. It is seen that the impact is noticeable for the larger relaxation time but is almost negligible for the smaller one. Because the exact value of τ_s is unknown, the thermal stress relaxation effect is excluded in all of the other calculations, including those already presented.

The stress humps in Fig. 6 occur around $x = 17$ nm at $t = 5.0$ ps, 33 nm at $t = 10.0$ ps, etc. The peak of the stress humps first increases with time, then rapidly decreases, and ultimately vanishes. For example, the values of the four peaks shown in Fig. 6 are -3.23, -4.17, -5.00, and -2.34 GPa at $t = 5.0$, 10.0, 15.0, and 20.0 ps, respectively. It is calculated, from the shift of the stress peaks, that the stress wave propagates with a speed close to the speed of sound in an extended medium, 3.14 km/s. The cause of the stress humps is essentially the hot-electron blast effect. This can be seen in Fig. 8, where the time history of stress σ_{xx} is computed with and without the hot-electron blast force B_x, respectively. Apparently, no stress humps occur at the first two time instants $t = 5.0$ and 10.0 ps when the hot-electron effect is neglected. Although the stress humps occur at the next two time instants $t = 15.0$ and 20.0 ps, their magnitudes are smaller. The difference between the two solutions is the response that results from the hot-electron blast force alone.

Because the response time of ultrafast laser heating is in picoseconds, thermal expansion in such a short period of time could result in a considerably high strain rate. In this work the calculated strain

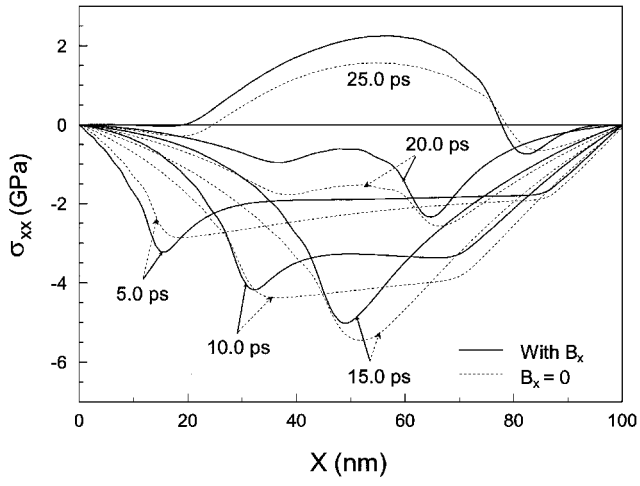

Fig. 8 Effect of hot-electron blast force on stress σ_{xx} in a 100-nm gold film heated by a laser pulse with $t_p = 100$ fs and $J_0 = 4000$ J/m^2.

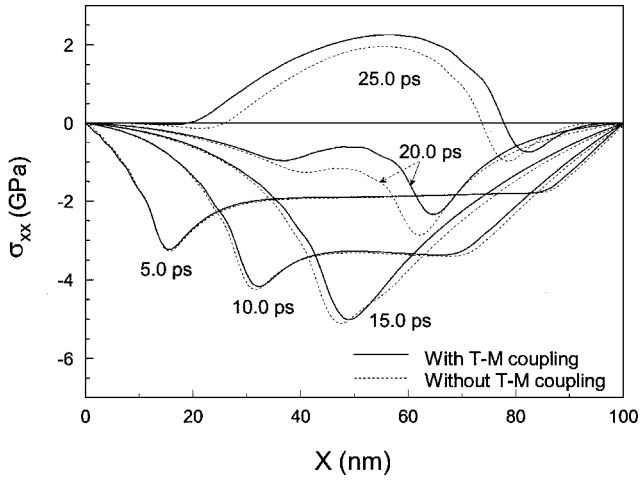

Fig. 9 Effect of thermal-mechanical coupling on stress σ_{xx} in a 100-nm gold film heated by a laser pulse with $t_p = 100$ fs and $J_0 = 4000$ J/m^2.

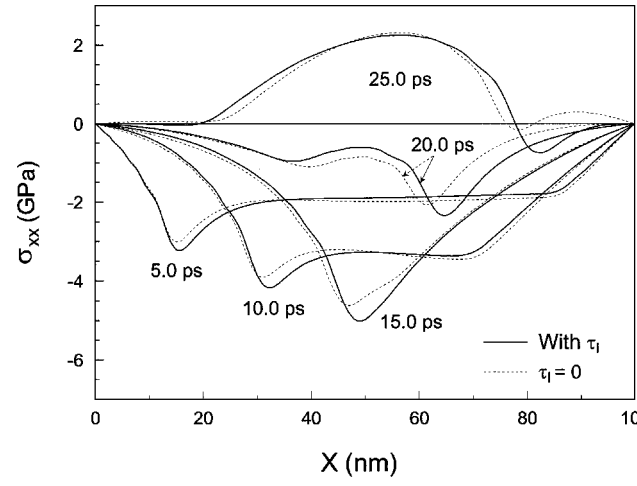

Fig. 10 Effect of phonon relaxation on stress σ_{xx} in a 100-nm gold film heated by a laser pulse with $t_p = 100$ fs and $J_0 = 4000$ J/m^2.

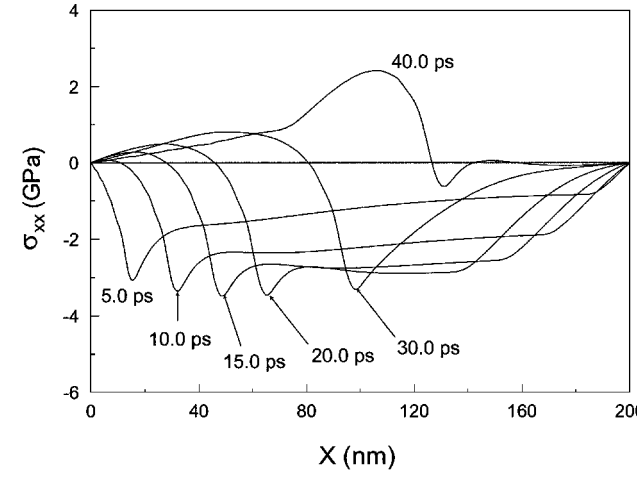

Fig. 11 Stress σ_{xx} distribution at different time instants in a 200-nm gold film heated by a laser pulse with $t_p = 100$ fs and $J_0 = 4000$ J/m^2.

rates are on the order of 10^9 s^{-1}; the actual values depends on the laser intensity. As a result of the high strain rate, the coupling effect between lattice temperature and strain rate might not be negligible. The numerical result shows that the coupling effect indeed affects the lattice temperature field. For instance, the first maximum lattice temperature at the irradiated surface is 1244 K occurring at $t = 29.03$ ps predicted with the coupling effect, whereas it is 1303 K occurring at $t = 31.07$ ps predicted without the effect. The relative difference of the two maximum temperatures is about 4.7%. Because of the change of the lattice temperature field, it is expected that the computed thermomechanical response would be different. Figure 9 shows the effect of thermal-mechanical (T-M) coupling on the thermal stress σ_{xx}. Evidently, the stress computed with the coupling effect differs from that computed without the effect, especially in late time.

The effect of the phonon relaxation on the stress response of σ_{xx} is depicted in Fig. 10. It is recalled that the phonon relaxation time is less temperature sensitive and is calculated to be 38.7 ps at room temperature, which is much longer than the laser pulse duration considered here. Like the coupling effect between lattice temperature and strain rate, the phonon relaxation effect certainly alters the lattice temperature and in turn the stress response although it hardly affects the electron temperature. However, in contrast to the T-M coupling effect, neglecting the phonon relaxation effect yields a smaller lattice temperature. For instance, the calculated first maximum lattice temperature at the front surface lessens to 1223 K, comparing to 1244 K computed with the effect. Because of the reduction in the lattice temperature, the magnitude of the resulting stress peaks becomes smaller, as seen in Fig. 10.

With the electron relaxation effect the calculated range of the electron temperature is 300 ~ 19,181 K. The corresponding electron relaxation time is 26 ~ 0.2 fs. The relative difference between the two maximum electron temperatures computed with and without the electron relaxation effect is only 0.2% (about 39 K). Consequently, the impact of the electron relaxation on the hot-electron blast force, lattice temperature, and thermal stress all are trivial. Because the laser pulse duration is quite long in comparison with the electron relaxation time, another pulse having a durations of $t_p = 10$ fs is studied. It is found that for this shorter pulse the maximum electron temperature increases to 21,776 K. The impact of the electron relaxation on the thermomechanical responses is more pronounced but is still limited.

Figure 11 shows the stress σ_{xx} distribution in a 200-nm film at several time instants. The hot-electron blast effect, again, is evidenced by the sharp stress pulses. By comparing the peaks of the stress pulses with the plateaus over the rest region at $t = 5.0$ and 10.0 ps in Figs. 6 and 11 respectively, it seems that the hot-electron blast effect is more significant for a 200-nm film than for a 100-nm film. A similar stress response is also found for the 400-nm film. Owing to the similarity, the results of the 400-nm film are not presented here.

The stress σ_{xx} distribution in a 50-nm film heated by a laser pulse with $t_p = 100$ fs and $J_0 = 2000$ J/m^2 is plotted in Fig. 12. Comparing the stress pulse profiles in Figs. 6, 11, and 12 makes it clearer that the thicker the film, the more pronounced the impact

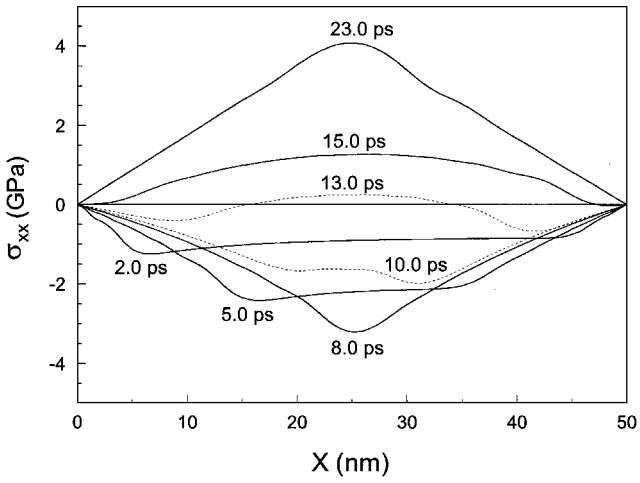

Fig. 12 Stress σ_{xx} distribution at different time instants in a 50-nm gold film heated by a laser pulse with $t_p = 100$ fs and $J_0 = 2000$ J/m^2.

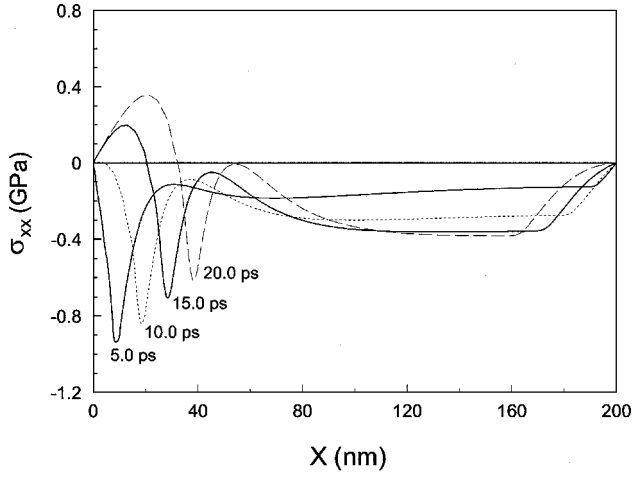

Fig. 13 Uniaxial stress σ_{xx} distribution at different time instants in a 200-nm gold film heated by a laser pulse with $t_p = 100$ fs and $J_0 = 4000$ J/m^2.

of the hot-electron blast effect. The reason is that it takes less time for the electron (and lattice also) temperature in a thinner film to achieve a uniform state than for that in a thicker film; as a result, the gradient of the electron temperature squared and in turn the hot-electron blast force [Eq. (8)] in a thinner film would be relatively small. The maximum compressive stress occurs in the middle region for the 50- and 100-nm films, but it occurs in the region near the front surface for the 200- and 400-nm films.

Figures 13 and 14 respectively represent the stress σ_{xx} in the 200- and 50-nm films, computed with the uniaxial stress assumption. Each loading condition is identical to that in the corresponding uniaxial strain case. From the location of the stress peaks given in Figs. 13 and 14, the calculated stress waves travel with a speed in a bounded medium, 1.97 km/s. It is also seen from Figs. 11–14 that the uniaxial stress condition results in less severe thermal stress than the uniaxial strain condition.

Detailed examination of Figs. 6–14 reveal that the discontinuities carried by the thermal [Eqs. (13) and (14)] and mechanical [Eqs. (10) and (20)] wavefronts are the dominating mechanisms in material failure caused by low-power ultrashort laser heating. A slow-moving front would destroy the film in its wake area, promoting tensile damage as the surface integrity is lost caused by rapid thermomechanical interactions. A fast-moving front at short times, on the other hand, produces discontinuities that bounce back and forth between the film surfaces. The resulting rapid alterations between tension and compression would accumulate significant hysteresis energy within the conductor, causing fatigue-like local failure under excessively

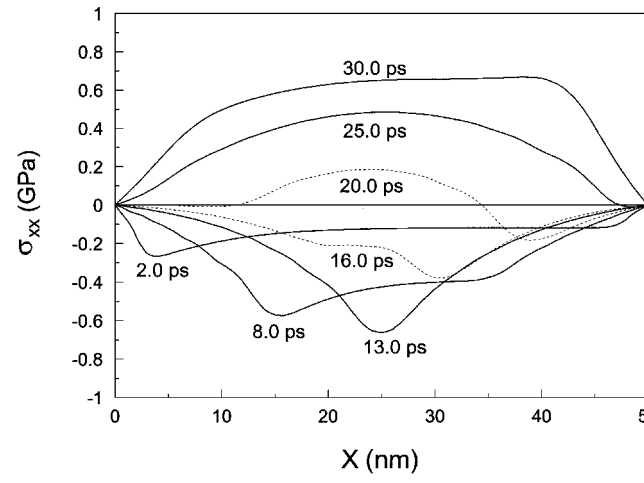

Fig. 14 Uniaxial stress σ_{xx} distribution at different time instants in a 50-nm gold film heated by a laser pulse with $t_p = 100$ fs and $J_0 = 2000$ J/m^2.

high frequencies.[26] These are possible failure modes in absence of the hydrodynamic motion of plasma.

Conclusions

This paper proposes an ultrafast thermoelasticity model to analyze the heat transport and thermomechanical phenomena in metal films irradiated by femtosecond laser pulses. It is found that the thermomechanical responses between the films thicker than 200 nm and those thinner than 100 nm are different. The thicker the films, the more pronounced the hot-electron blast effect. The maximum compressive stress occurs in the middle region for the films thinner than 100 nm but in the region near the heated surface for the films thicker than 200 nm. The effect of thermal stress relaxation on the thermomechanical response might be vital only for a small range of the relaxation time, somewhere around the one-hundredth of the phonon relaxation time. The electron relaxation effect is inconsequential for the lasers available to date. On the other hand, the effect of phonon thermal relaxation is important when a laser pulse duration is comparable to or shorter than the phonon relaxation time. Because the strain rate is extremely high, on the order of 10^9 s^{-1}, the coupling effect between thermal and mechanical energy in the lattice is also important. Under the same loading condition the uniaxial strain condition results in much more severe thermal stresses than the uniaxial stress condition.

Ultrafast deformation in metal lattices induced by the hot electron blast is an important physical mechanism activated in the picosecond domain. Optimal operating conditions to prevent thermomechanical failure in general, however, have a much larger scope that requires further integration of other physical mechanisms into the analytical model, including the plasma formation and expansion during the short-time transient. Though complicated, interactions of pressure waves induced by the plasma expansion and the hot-electron blast should be an interesting topic of research in ultrafast thermomechanics.

References

[1] Preuss, S., Matthias, E., and Stuke, M., "Sub-Picosecond UV-Laser Ablation of Ni Films: Strong Fluence Reduction and Thickness-Independent Removal," *Applied Physics A*, Vol. 59, No. 1, 1994, pp. 79–82.

[2] Preuss, S., Demchuk, A., and Stuke, M., "Sub-Picosecond UV Laser Ablation of Metals," *Applied Physics A*, Vol. 61, No. 1, 1995, pp. 31–37.

[3] Pronko, P. P., Dutta, S. K., Squier, J., Rudd, J. V., Du, D., and Mourou, G., "Machining of Sub-micron Holes Using a Femtosecond Laser at 800 nm," *Optics Communications*, Vol. 114, Nos. 1, 2, 1995, pp. 106–110.

[4] Staurt, B. C., Feit, M. D., Herman, S., Rubenchik, A. M., Shore, B. W., and Perry, M. D., "Optical Ablation by High-Power Short-Pulse Lasers," *Journal of the Optical Society of America*, Vol. 13, No. 2, 1996, pp. 459–468.

[5] Momma, C., Nolte, S., Chichkov, B. N., Alvensleben, F. V., and Tunnermann, A., "Precise Laser Ablation with Ultrashort Pulses," *Applied Surface Science*, Vol. 109, 1997, pp. 15–19.

[6]Lenzner, M., Kruger, J., Kautek, W., and Krausz, F., "Precision Laser Ablation of Dielectrics in the 10-fs Regime," *Applied Physics A*, Vol. 68, No. 3, 1999, pp. 369–371.

[7]Perry, M. D., Staurt, B. C., Banks, P. S., Feit, M. D., Yanovsky, V., and Rubenchik A. M., "Ultrashort-Pulse Laser Machining of Dielectric Materials," *Journal of Applied Physics*, Vol. 85, No. 9, 1999, pp. 6803–6810.

[8]Falkovsky, L. A., and Mishchenko, E. G., "Electron-Lattice Kinetics of Metals Heated by Ultrashort Laser Pulses," *Journal of Experimental and Theoretical Physics*, Vol. 88, No. 1, 1999, pp. 84–88.

[9]Welsh L. P., Tuchman, J. A., and Herman, I. P., "The Importance of Thermal Stresses and Strains Induced in Laser Processing with Focused Gaussian Beams," *Journal of Applied Physics*, Vol. 64, No. 11, 1988, pp. 6274–6286.

[10]Cohen, S. S., Bernstein, J. B., and Wyatt, P. W., "The Effect of Multiple Pulse on Damage to Thin Metallic Films," *Journal of Applied Physics*, Vol. 71, No. 2, 1992, pp. 630–637.

[11]Chandrasekharaiah, D. S., and Srinath, K. S., "Thermoelastic Plane Waves Without Energy Dissipation in a Half-Space Due to Time-Dependent Heating of the Boundary," *Journal of Thermal Stresses*, Vol. 20, No. 7, 1997, pp. 659–676.

[12]Tehrani, P. H., Hector, L. G., Jr., Hetnarski, R. B., and Eslami, M. R., "Boundary Element Formulation for Thermal Stresses During Pulsed Laser Heating," *Journal of Applied Mechanics*, Vol. 68, No. 3, 2001, pp. 480–489.

[13]Lord, H. W., and Shulman, Y., "A Generalized Dynamic Theory of Thermoelasticity," *Journal of Mechanics and Physics in Solids*, Vol. 15, No. 5, 1967, pp. 229–309.

[14]Green, A. E., and Lindsay, K. A., "Thermoelasticity," *Journal of Elasticity*, Vol. 2, No. 1, 1972, pp. 1–7.

[15]Green, A. E., and Naghdi, P. M., "Thermoelasticity Without Energy Dissipation," *Journal of Elasticity*, Vol. 31, No. 2, 1993, pp. 189–208.

[16]Hetnarski, R. B., and Ignaczak, J., "Soliton-Like Waves in a Low-Temperature Nonlinear Thermoelastic Solids," *International Journal of Engineering Science*, Vol. 34, No. 15, 1996, pp. 1767–1787.

[17]Tzou, D. Y., *Macro- to Microscale Heat Transfer: The Lagging Behavior*, Taylor and Francis, Washington, DC, 1997, pp. 259–264.

[18]Chandrasekharaiah, D. S., "Hyperbolic Thermoelasticity: A Review of Recent Literature," *Applied Mechanics Review*, Vol. 51, 1998, pp. 705–729.

[19]Hetnarski, R. B., and Ignaczak, J., "Generalized Thermoelasticity," *Journal of Thermal Stresses*, Vol. 22, No. 4, 1999, pp. 451–476.

[20]Hetnarski, R. B., and Ignaczak, J., "Nonclassical Dynamical Thermoelasticity," *International Journal of Solid and Structures*, Vol. 37, Nos. 1, 2, 2000, pp. 215–224.

[21]Enguehard, F., and Betrand, L., "Effects of Optical Penetration and Laser Pulse Duration on Laser Generated Longitudinal Acoustic Waves," *Journal of Applied Physics*, Vol. 82, No. 4, 1997, pp. 1532–1538.

[22]Juh, C. S., and Burger, C. P., "Effects of Thermomechanical Coupling and Relaxation Times on Wave Spectrum in Dynamic Theory of Generalized Thermoelasticity," *Journal of Applied Mechanics*, Vol. 65, No. 3, 1998, pp. 605–613.

[23]Tehrani, P. H., and Eslami, M. R., "Boundary Element Analysis of Coupled Thermoelasticity with Relaxation Times in Finite Domain," *AIAA Journal*, Vol. 38, No. 3, 2000, pp. 534–541.

[24]Wang, X., and Xu, X., "Thermoelastic Wave Induced by Pulsed Laser Heating," *Applied Physics A*, Vol. 73, 2001, pp. 107–114.

[25]Anisimov, S. I., Kapeliovich, B. L., and Perel'man, T. L., "Electron Emission from Metal Surfaces Exposed to Ultra-Short Laser Pulses," *Soviet Physics Journal of Experimental and Theoretical Physics*, Vol. 39, No. 2, 1974, pp. 375–377.

[26]Chen, P., Tomov, I. V., and Rentzepis, P. M., "Crystal Stress Dynamics by Means of Nanosecond Time-Resolved X-Ray Diffraction," *Applied Physics Letter*, Vol. 71, No. 12, 1997, pp. 1646–1652.

[27]Chen, P., Tomov, I. V., and Rentzepis, P. M., "Time-Resolved Heat Propagation in a Gold Crystal by Means of Picosecond X-Ray Diffraction," *Journal of Chemical Physics*, Vol. 104, No. 24, 1996, pp. 10,001–10,007.

[28]Tzou, D. Y., Chen, J. K., and Beraun, J. E., "Ultrafast Deformation in Femtosecond Laser Heating," *Journal of Heat Transfer*, Vol. 124, No. 2, 2002, pp. 284–292.

[29]Chen, J. K., Beraun, J. E., and Tzou, D. Y., "Thermomechanical Response of Metals Heated by Ultrafast-Pulsed Lasers," *Journal of Thermal Stresses*, Vol. 25, No. 6, 2002, pp. 539–558.

[30]Chen, J. K., and Beraun, J. E., "Numerical Study of Ultrashort Laser Pulse Interactions with Metal Films," *Numerical Heat Transfer Part A: Applications*, Vol. 40, No. 1, 2001, pp. 1–20.

[31]Boley, B. A., and Weiner, J. H., *Theory of Thermal Stresses*, Wiley, New York, 1960, pp. 1–40.

[32]Qiu, T. Q., and Tien, C. L., "Heat Transfer Mechanisms During Short-Pulse Laser Heating of Metals," *Journal of Heat Transfer*, Vol. 115, No. 4, 1993, pp. 835–841.

[33]Kittle, C., *Introduction to Solid State Physics*, Wiley, New York, 1967, pp. 207–214.

[34]Hector, L. G., Jr., and Hetnarski, R. B., "Thermal Stresses in Materials Due to Laser Heating," *Thermal Stress IV*, edited by R. B. Hetnarski, Elsevier, Amsterdam, 1996, Chap. 6, pp. 454–532.

[35]Hetnarski, R. B., and Ignaczak, J., "Generalized Thermoelasticity: Response of Semi-Space to a Short Laser Pulse," *Journal of Thermal Stresses*, Vol. 17, No. 3, 1994, pp. 377–396.

[36]Hector, L. G., Jr., and Hetnarski, R. B., "Thermal Stresses Due to a Laser Pulse: The Elastic Solution," *Journal of Applied Mechanics*, Vol. 63, No. 1, 1996, pp. 38–46.

[37]Kim, W. S., Hector, L. G., Jr., and Hetnarski, R. B., "Thermoelastic Stresses in a Bonded Layer Due to Repetitively Pulsed Laser Radiation," *Acta Mechanica*, Vol. 125, No. 1, 1997, pp. 107–128.

[38]Qiu, T. Q., and Tien, C. L., "Short-Pulse Laser Heating on Metals," *International Journal of Heat and Mass Transfer*, Vol. 35, No. 3, 1992, pp. 719–726.

[39]Qiu, T. Q., and Tien, C. L., "Femtosecond Laser Heating of Multi-Layered Metals—I. Analysis," *International Journal of Heat and Mass Transfer*, Vol. 37, No. 17, 1994, pp. 2789–2797.

[40]Qiu, T. Q., Juhasz, T., Suarez, C., Bron, W. E., and Tien, C. L., "Femtosecond Laser Heating of Multi-Layered Metals—II. Experiments," *International Journal of Heat and Mass Transfer*, Vol. 37, No. 17, 1994, pp. 2799–2808.

[41]Wang, X. Y., Riffle, D. M., Lee, Y. S., and Downer, M. C., "Time-Resolved Electron-Temperature Measurement in a Highly Excited Gold Target Using Femtosecond Thermionic Emission," *Physics Review B*, Vol. 50, No. 11, 1994, pp. 8016–8019.

[42]Anismov, S. I., and Rethfeld, B., "On the Theory of Ultrashort Laser Pulse Interaction with Metal," *SPIE*, Vol. 3093, 1997, pp. 192–203.

[43]Anderson, D. A., Tannehill, J. C., and Pletcher, R. H., *Computational Fluid Mechanics and Heat Transfer*, McGraw–Hill, New York, 1984, pp. 167–172.

[44]Meyers, M. A., *Dynamic Behavior of Materials*, Wiley, New York, 1994.

[45]Touloukian, Y. S., Powell, R. W., Ho, C. Y., and Klemens, P. G., *Thermal Conductivity, Thermopyhsical Properties of Matter*, Vol. 1, IFI/Plenum, New York, 1970, pp. 135–137.

[46]Touloukian, Y. S., and Buyco, E. H., *Specific Heat, Thermopyhsical Properties of Matter*, Vol. 4, IFI/Plenum, New York, 1970, p. 85.

[47]Trent, H. M., Stone, D. E., and Beraubien, L. A., "Elastic Constants, Hardness, Strength, Elastic Limits, and Diffusion Coefficients of Solids," *American Institute of Physics Handbook*, edited by D. E. Gary, McGraw–Hill, New York, 1972, pp. 2–60.